Neuroscience Letters (Accepted 13 Feb 2023). https://doi.org/10.1016/j.neulet.2023.137133

Recognition of unilateral lower limb movement based on EEG signals with ERP-PCA analysis

Lingyun Gu[a,+], Jiuchuan Jiang[b,+], Hongfang Han[a], John Q. Gan[c], Haixian Wang[a,*]

[a] Key Laboratory of Child Development and Learning Science of Ministry of Education, School of Biological Science & Medical Engineering, Southeast University, Nanjing 210096, Jiangsu, PR China

[b] School of Information Engineering, Nanjing University of Finance and Economics, Nanjing 210003, Jiangsu, PR China

[c] School of Computer Science and Electronic Engineering, University of Essex, Colchester CO4 3SQ, UK

+ Co-first authors.

* Corresponding author. E-mail addresses: hxwang@seu.edu.cn

Abstract:

It has been confirmed that motor imagery (MI) and motor execution (ME) share a subset of mechanisms underlying motor cognition. In contrast to the well-studied laterality of upper limb movement, the laterality hypothesis of lower limb movement also exists, but it needs to be characterized by further investigation. This study used electroencephalographic (EEG) recordings of 27 subjects to compare the effects of bilateral lower limb movement in the MI and ME paradigms. Event-related potential (ERP) recorded was decomposed into meaningful and useful representatives of the electrophysiological components, such as N100 and P300. Principal components analysis (PCA) was used to trace the characteristics of ERP components temporally and spatially, respectively. The hypothesis of this study is that the functional opposition of unilateral lower limbs of MI and ME should be reflected in the different alterations of the spatial distribution of lateralized activity. Meanwhile, the significant ERP-PCA components of the EEG signals as identifiable feature sets were applied with support vector machine to identify left and right lower limb movement tasks. The average classification accuracy over all subjects is up to 61.85% for MI and 62.94% for ME. The proportion of subjects with significant results are 51.85% for MI and 59.26% for ME, respectively. Therefore, a potential new classification model for lower limb movement can be applied on brain computer interface (BCI) systems in the future.

Key words: lower limb, motor imagery, motor execution, principal components analysis.

1 | Introduction

Brain-computer interface (BCI) systems, for the sake of directly transmitting messages from the human brain to computers based on the brain's mental activities, have grown rapidly in the last three decades [1-3]. EEG based BCI systems have unique advantages such as non-invasive, high time resolution, and affordable [4]. Motor imagery (MI), as one of the most widely used cognitive tasks, can be defined as sending a command to a BCI system by the user through the imagination of a limb movement. Compared to motor execution (ME), MI shares many commonalities in terms of performance and underlying neural substrates, which means that they share the cortical networks involving the contralateral BA4, PMd, parietal areas and SMA [5]. Based on the neural simulation theory, Jeannerod [6] has stated that motor imagery (MI) is a covert action that differs from an overt action only in that the action is not executed. This is the so-called 'functional equivalence' [7-10]. However, functional equivalence does not mean identical. In some neuroimaging studies, the functional activation patterns of the two types of movements are different [11, 12]. Therefore, it is essential to investigate whether the similarity extends to the specific type of limb movement. This is helpful for BCI systems to realize more refined motion control.

This paper focuses on identification of the unilateral lower limb movement. Packheiser, et al. [13] have made a general statement that lower limb movement is lateralized through meta-analyses for footedness over 100k individuals across 164 studies. Besides, many studies of unilateral limb movement have confirmed that some effective components [14, 10, 15] of EEG can reflect the lateralization. The high identification rate of these laterality components can further guide the design of BCI systems to achieve accurate control. Due to the lack of research on the unilateral lower limb movement based on the general ERP components such as N1 and P3, the effective ERP components should be found to describe the left-right difference of the lower limb movement and verify the validity of these features in the classification model. Moreover, for developing lower limb MI-BCI systems, spatiotemporal features of single-trials are extracted from the ERP-PCA components to reduce the dimension of complex signals.

This study aims to: (1) analyze the temporal ERP components in ME and MI of the unilateral lower limb; (2) investigate the differences between left and right foot movements (including ME and MI) with two-step ERP-PCA; (3) provide a novel BCI design for classifying left and right foot movements from EEG signals.

2 | Materials and methods

2.1 | Participants and ethics statement

Twenty-seven right-handed volunteers (eleven females) without a history of neuromuscular disorders took part in this study. All participants had normal or corrected-to-normal vision. The mean age of participants was 24.52 (SD=1.52) years. The Ethical Committee of Southeast University, Nanjing, China gave approval to the project, and the study has complied with the Declaration of Helsinki. Each participant signed the informed consent prior to participation and was paid 150 RMB as a reward.

2.2 | Lower limb movement tasks and procedure

A version of the lower limb movement task used by Yasunari and Junichi [15] has two conditions: real foot movement and imaginary foot movement. Each condition of foot movement consists of two tasks, including left and right foot movement. Stimuli display was controlled by E-prime v.2 (Psychology Software Tools, http://www.pstnet.com). During the ME part, the subject dorsiflexed a foot and maintained movements for 1 second (brisk movement). During the MI part, the subject was instructed to use kinaesthetic rather than visual imagery.

Two kinds of foot movements (ME and MI) consist of five cue-based sessions, which were performed respectively. Each session consists of 30 trials, with 15 trials for the left foot and 15 trials for the right foot in random order. There was a 3-minute rest period between sessions. Besides, the ME was conducted before the MI. There was a 7-minute

rest period between ME and MI sessions. The experimental paradigm of the cue-based session is shown in Figure 1. With different combinations of conditions (ME and MI) and sides (Left and Right), there are 4 tasks: (a) Left foot motor execution (LFME), (b) Right foot motor execution (RFME), (c) Left foot motor imagery (LFMI), and (d) Right foot motor imagery (RFMI).

FIGURE 1 Experimental procedure. An arrow indicates right or left lower limb movement task.

2.3 | Electroencephalogram recording and pre-processing

Continuous EEG activity was acquired from a 64-channel Synamps amplifier (NeuroScan, version 4.3) by using the electrodes mounted in an elastic cap according to the International 10-20 system and referenced to the right earlobe. The vertical EOG signals and horizontal EOG signals were recorded. Electrode impedances were kept below 5 kΩ. The sampling rate was 1,000 Hz with a 0.3 to 70 Hz bandpass filter.

Signal pre-processing was conducted in MATLAB (Mathworks Inc.). EEG recordings were filtered at 0.5-40 Hz with IIR filter. Independent Component Analysis (ICA) was performed using the EEGLAB toolbox [16]. The components were inspected by Adjust tool and contaminated components, corresponding mainly to ocular artifacts, were rejected. The epochs were set from 1000 ms pre-stimulus to 1500 ms post-stimulus. Consequently, this produced four sets of artifact datasets. Each participant produced less than 75 trials (15*5 sessions) for each task. A total of 2020 trials for LFME, 2022 trials for REMI, 2025 trials for LFMI, and 2025 trials for RFMI were selected for further analysis.

2.4 | Data analysis

2.4.1 | Temporospatial analysis

The ERP PCA Toolkit [17] was used to reconstruct the factor waveforms and apply inferential statistics. The ts-PCA was recommended by [18] to reduce the dimensionality and separate the meaningful ERP components. For the temporal-PCA (t-PCA), the input was the average of all epochs for each task of every subject. There were 6480 cases (27 participants* 60 channels*4 conditions) and 2,500 variables (-1000 to 1500 ms data sampled to 1,000 Hz). The new set of ERPs, which was obtained from the set of temporal factors, was submitted to a spatial-PCA (s-PCA). The characteristic spatial patterns can be extracted from the virtual electrode corresponding to the temporal component, which was treated as virtual ERPs.

2.4.2 | Statistical analysis

ERP components from the t-PCA were analyzed using mean amplitude in the selected time windows pooled from electrode clusters. The electrodes contained in the clusters were shown in Figure 2. Three-way robust ANOVA (condition * side * region) was used to assess the difference in ERP components. For the s-PCA, robust ANOVAs

were used to conduct a two-way ANOVA (condition * side). Familywise corrected alpha criteria of 0.05 and the Dunn-Šidák MCP correction for post-hocs were used in robust ANOVA.

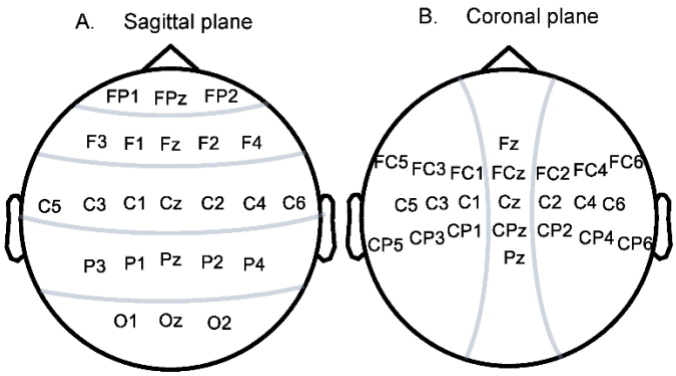

FIGURE 2 Electrode clusters. (A) Sagittal plane: frontal pole region including Fp1, Fpz, Fp2, frontal region including F3, F1, Fz, F2, F4, central region including C3, C1, Cz, C2, C4, and parietal region including P3, P1, Pz, P2, P4, and occipital region including O1, Oz, O2. (B) Coronal plane: left region including F3, C3, P3, midline region including Fz, Cz, Pz, and right region including F4, C4, P4.

2.5 | Feature selection and classification

Let a multichannel ERP time series be represented as an $m \times n$ matrix X_{ERP}, where m is the number of channels and n is the number of time samples. A singular value decomposition (SVD) of X_{ERP} yields

$$X_{ERP} = USV^{\mathrm{T}} = \sum_{i=1}^{d} \lambda_i u_i v_i^{\mathrm{T}} \tag{1}$$

where $U = [u_1, u_2, \ldots, u_h]$ and $V = [v_1, v_2, \ldots, v_g]$ are orthogonal matrices, Σ is a diagonal matrix with nonnegative λ_i along the diagonal in decreasing order, d=rank(X_{ERP}) is the number of nonzero singular values, λ_i is the i-th largest singular value of X_{ERP}, and the vector $u_i(v_i)$ is the i-th left(right) singular vector.

For classification, a spatial-temporal feature matrix of the EEG signals X_{EEG} is defined as

$$F_{\mathrm{TS}} = U^{l^*} X_{\mathrm{EEG}} (V^{l^*})^{\mathrm{T}} \tag{2}$$

where V^{l^*} is a significant spatial vector, U^{l^*} is a significant temporal vector, and F_{TS} is a $l \times l$ matrix. Support vector machine (SVM) as a classifier is simple, robust, accurate, and efficient to obtain satisfactory results [19, 20]. Therefore, a binary SVM classifier was used to differentiate the effective features between the left and right motor tasks of two conditions. A 10-fold cross-validation procedure was performed on two feature-sample sets. Linear kernel function (LKF) was selected. The permutation test was applied to ensure the significance of classification results. The surrogated times of the permutation test is 1000.

3 | Results

3.1 | t-PCA ERP analysis

The t-PCA with unrestricted Promax rotation was used for the four tasks, which yielded 7 identifiable factors with over 1.0% variance. The t-PCA results of subject#9 are shown in Figure 3. The t-PCA N100 and P300 component waveforms at C3 (left hemisphere), C4 (right hemisphere), and Pz (midline site) in the curve section were almost consistent with the mean ERPs in terms of latency and amplitude. Combined with the table section

below, it is easy to find that a large N100 peaks at around 180 ms in the ERP waveforms for each condition, followed by a large P300 peaking at around 350ms. Furthermore, a similar distribution shown in topography section was found in the N100 and P300 components in the four tasks, which includes a centraltoparietal N100 and a parietal P300. It should be pointed out that P300 components were obviously present in the ERPs of all subjects and the N100 component was not present in three subjects (subjects#4, subjects#15, and subjects#22).

The seven-factor t-PCA components were tested using a three-way robust ANOVA with *Condition* (ME, MI), *Side* (L, R), and *Region* (as shown in Figure 2). The components were arranged in descending order of variance (TF1, TF2, TF3, TF4, TF5, TF6, and TF7). The results are shown in Table 1a. There was a significant condition of TF7, confirming that across *Side* and *Region* the pattern of activity was different per condition. And there was a significant region of TF2 and TF4, verifying that across *Condition* and *Side* each region had a different pattern of activity. Furthermore, the post-hoc test for each of the regions was shown in Table 1b. This region effect of TF2 was restricted to the Frontal site and Middle sites. The post-hoc result of TF4 shows that most brain sites were significant, leading to the significance of the region as the main effect.

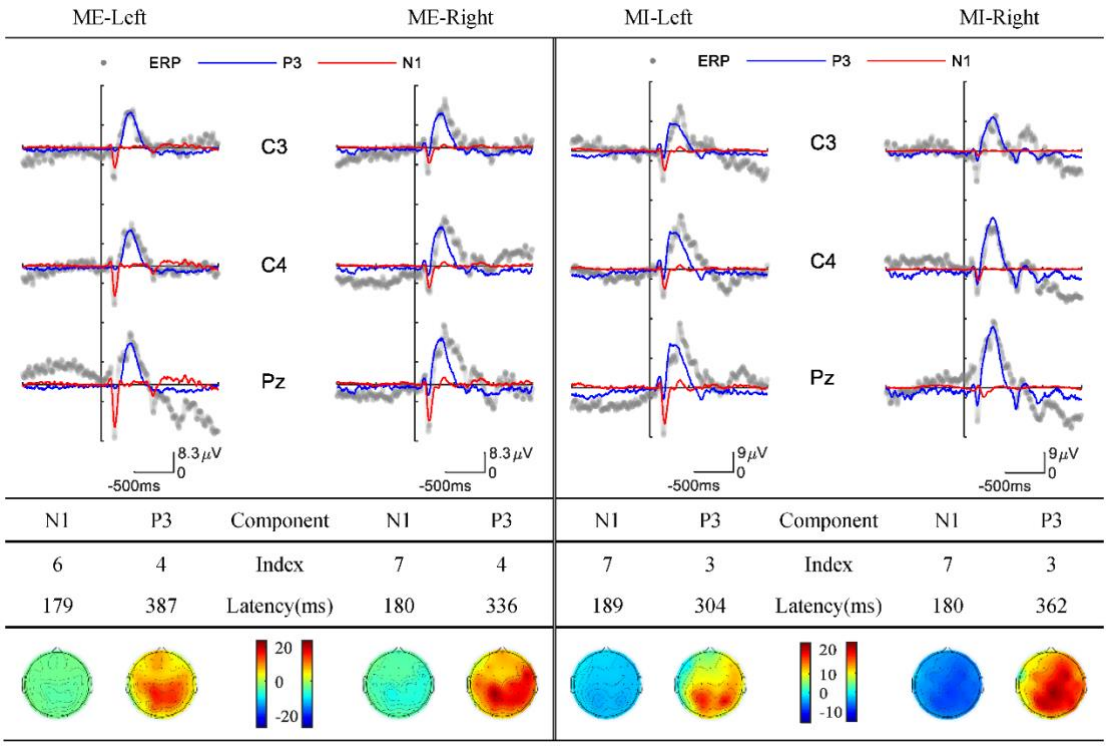

FIGURE 3 The t-PCA result of subject#9. A) The curve chart section shows mean ERPs and t-PCA derived N1 and P3 component waveforms for left and right foot tasks of real and imagery movement conditions. Each subgraph was plotted at C3, C4, and Pz from top to bottom. B) The table section in the middle shows the corresponding t-PCA derived N1 and P3 component information, including the index and the latency of the N1 and P3 components. C) The topography section shows the peak amplitude distribution of N1 and P3 components over all electrodes.

TABLE 1a Statistical test results for the t-PCA ERP components with Promax

	TF1		TF2		TF3		TF4		TF5		TF6		TF7	
Effect	T_{wjt}/c	P	T_{wjt}/c	P	T_{wjt}/c	P	T_{wjt}/c	P	T_{wjt}/c	P	T_{wjt}/c	P	T_{wjt}/c	P
C	3.560	0.076	1.530	0.240	0.950	0.336	2.040	0.170	3.330	0.079	0.170	0.690	6.660	**0.014***
S	0.160	0.710	0.000	0.950	0.110	0.740	0.010	0.941	0.310	0.590	0.260	0.610	0.430	0.530
R	5.680	0.054	10.300	**0.003****	2.300	0.280	15.380	**0.000****	4.080	0.053	2.260	0.180	4.060	0.088
C*S	0.030	0.870	0.430	0.525	0.990	0.340	0.990	0.360	0.020	0.900	0.050	0.820	1.060	0.330
C*R	1.780	0.370	3.540	0.130	1.220	0.526	2.710	0.150	0.960	0.607	0.950	0.630	1.510	0.477
S*R	1.390	0.490	0.610	0.880	1.090	0.580	0.630	0.790	3.480	0.095	1.890	0.320	1.210	0.500
C*S*R	3.850	0.130	1.740	0.430	1.390	0.490	1.220	0.590	1.200	0.606	1.010	0.554	1.320	0.470

*Note: C represents Condition (ME and MI). S represents Side (Left and Right). R represents Region. *(p<0.05), **(p<0)*

TABLE 1b Post-hoc results for the effect of Region

	TF2		TF4	
Effect	T_{wjt}/c	P	T_{wjt}/c	P
C vs F	6.830	**0.016***	54.960	**0.000****
C vs P	0.110	0.741	14.490	**0.001****
C vs O	1.350	0.260	4.230	**0.048***
C vs FP	38.860	**0.000****	1.470	0.230
F vs P	8.410	**0.008****	22.650	**0.000****
F vs O	7.420	**0.012***	29.910	**0.000****
F vs FP	0.300	0.590	30.310	**0.000****
P vs O	3.690	0.069	36.760	**0.000****
P vs FP	2.660	0.120	44.300	**0.000****
O vs FP	9.160	**0.011***	49.920	**0.000****
L vs R	0.370	0.550	0.330	0.570
L vs M	15.930	**0.001****	4.430	**0.047***
M vs R	17.030	**0.001****	1.280	0.280

3.2 | ts-PCA ERP analysis

The same number of factors was used for each of the s-PCAs, which yielded 6 identifiable factors with 1.0% variance. The N100 and P300 components of subject#9 at the first factor which was computed by s-PCA, including component waveforms and ts-PCA factor values, are shown in Figure 4. The N100 data are presented in Figure 4A and P300 in Figure 4B. The results of N100 and P300 were consistent with that of t-PCA, indicating that these two cognitive components were present in most electrodes. Observing the ts-PCA factors in Figure 5C, the P300 component of RFMI with the negative ts-PCA factor was different from the other tasks.

Each temporal factor has six spatial factors, so 42 temporal-spatial components were formed. Each component was tested using a two-way robust ANOVA with *Condition* and *Side*. The spatial components were arranged in descending order of variance (SF1, SF2, SF3, SF4, SF5, and SF6). The significant result is shown in Table 2. As the ERP components were mapped onto six virtual electrodes, the important results from this analysis only involve conditions and sides. There was a significant condition of TF4SF3, TF4SF6, TF5SF5, and TF6SF1, confirming that across tasks the pattern of activity was different per condition. Furthermore, there

was a significant condition by side interaction of TF2SF5 and TF4SF5. Marvelously, there was a significant side of TF2SF4, TF2SF5, TF5SF6, TF6SF2, and TF7SF2, verifying that across *Condition* the distribution of activity differed between the sides.

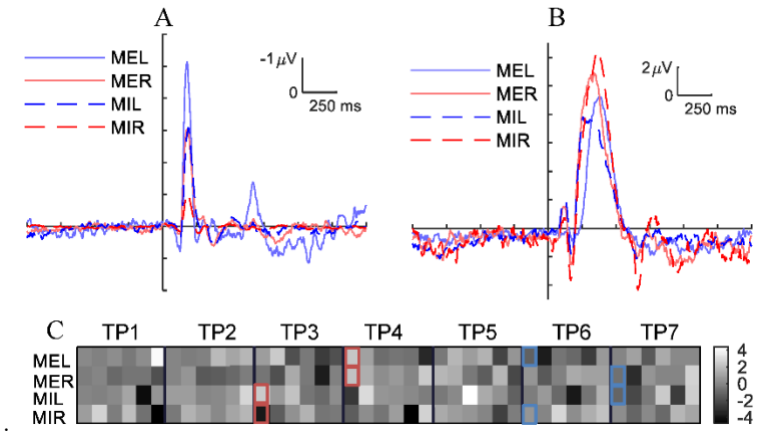

FIGURE 4 Mean ERPs of virtual channels (SF1) of subject#9 with ts-PCA. A) N100 component waveforms for left and right foot tasks of real and imagery movement conditions (MEL, MER, MIL, and MIR). B) P300 component waveforms of four tasks. C) Temporal-spatial PCA factors of four tasks from ts-PCA. The red rectangles represent the P300 component and the blue rectangles represent the N100 component.

TABLE 2 Statistical test results for the ts-PCA ERP components with ICA

	TF2SF4		TF2SF5		TF4SF3		TF4SF5		TF4SF6		TF5SF5	
	Twjt/c	p	Twjt/c	p	Twjt/c	p	Twjt/c	p	Twjt/c	p	Twjt/c	p
C	0.610	0.470	0.550	0.473	6.560	**0.019***	1.370	0.260	4.840	**0.033***	12.060	**0.002****
S	5.730	**0.019***	5.810	**0.037***	0.020	0.880	0.130	0.720	3.430	0.072	1.360	0.260
C*S	1.520	0.220	4.860	**0.046***	3.070	0.094	6.550	**0.018***	0.060	0.810	0.000	0.980
	TF5SF6		TF6SF1		TF6SF2		TF7SF2					
	Twjt/c	p	Twjt/c	p	Twjt/c	p	Twjt/c	p				
C	0.020	0.890	15.960	**0.001****	3.860	0.057	0.870	0.360				
S	14.550	**0.003****	0.330	0.590	7.190	**0.014***	8.200	**0.025***				
C*S	0.150	0.726	1.010	0.321	1.270	0.270	4.620	0.123				

*Note: C represents Condition (ME and MI). S represents Side (Left and Right). *(p<0.05), **(p<0.01)*

3.3 | Feature selection and classification

To classify the left and right motor tasks under each condition, seven-factor t-PCA and six-factor s-PCA were applied in each trial. Therefore, the size of the feature set formed in this way is 7 TFs × 6 SFs × *n* trials × *m* subjects × 4 tasks. The pair-T test with Bernoulli correction was applied to analyze the differences between the left and right motor tasks under ME and MI conditions respectively. The statistical test result is shown in Figure 5. It is easy to find that there are 7 PCA elements of ME condition with significant difference, which are TF4SF4 (22), TF4SF6 (24), TF5SF6 (30), TF6SF2 (32), TF7SF2 (38), TF7SF4 (40), TF7SF5 (41). Meanwhile, 9 PCA elements of MI condition with significant difference are TF2SF3 (9), TF3SF1 (13), TF3SF3 (15), TF3SF5 (17), TF4SF4 (22),

TF4SF6 (24), TF5SF3 (27), TF5SF4 (28), TF6SF3 (33).

Furthermore, Figure 6 and Table 3 present the validation accuracy of each subject with the permutation test. Significant classification results were obtained for 16 of the 27 subjects (59.26%) in the ME task and 14 of 27 subjects (51.85%) in the MI task in this dataset respectively. The average accuracy of classification was up to 62.94% and 61.85% in two conditions respectively. The proportion of subjects with good classification results under both conditions is 37.04%. Furthermore, a reliability test was conducted on the classification results at the individual level and the value of Cronbach's alpha was 0.919 (>0.7). The classification accuracy at the population level was significantly greater than 50% in each *Condition*.

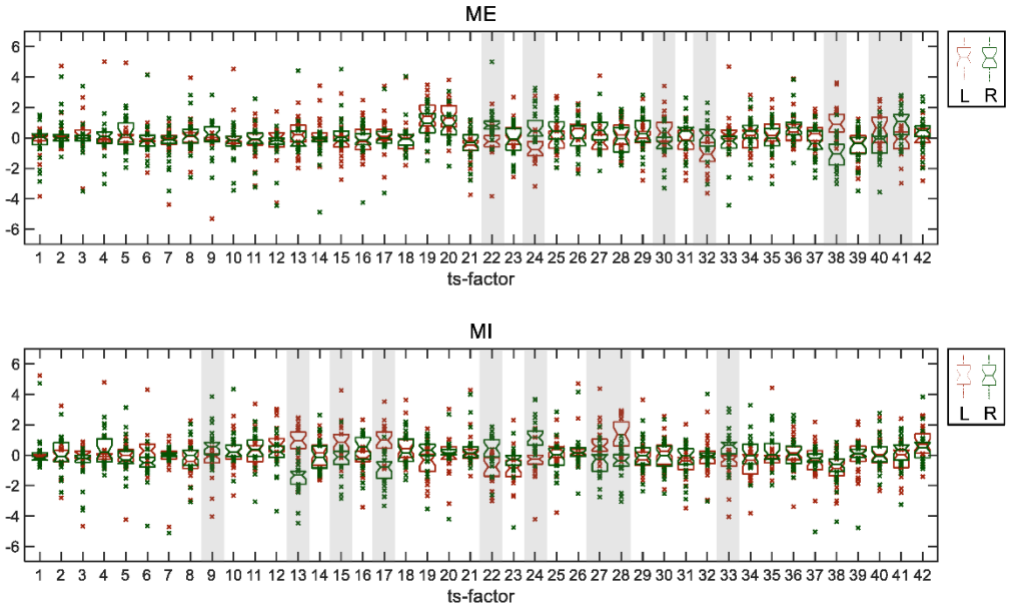

FIGURE 5 Pair-T test result of left and right motor task of ts-PCA factors over each condition (ME, MI). The transparent rectangle indicates the significant ts-PCA factors.

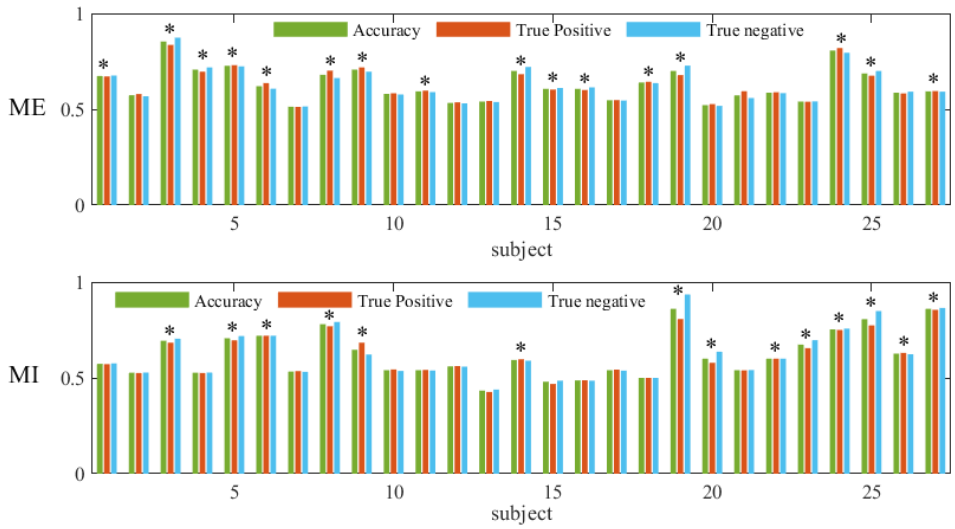

FIGURE 6 Accuracy of classification of each subject.*(p<0.05)

TABLE 3 The mean accuracy of classification

	ME			MI		
	ACC (%)	TP (%)	TN (%)	ACC (%)	TP (%)	TN (%)
Mean (std)	62.94(0.08)	63.03(0.08)	63.00(0.09)	61.85(0.12)	61.37(0.11)	62.57(0.13)
*Mean (std)	68.13(7.37)	68.02(7.22)	68.40(7.78)	70.86(9.27)	69.99(8.38)	72.20(10.69)
Population level	58.89	59.30	58.52	59.38	59.01	59.78

*Note: ACC represents accuracy, TP represents True Positive, which means the proportion of the correct left foot label in the all left labels. TN represents True Negative, which means the proportion of the correct right foot label in the all right labels, *mean (std) represents average accuracy of the significant subjects. Population level represents the average accuracy of all subjects.*

4 | Discussions

BCI can implement brain state-dependent control of robotic devices to help stroke patients for rehabilitation. This paper especially focuses on investigating the unilateral movement of the lower extremities. It tried to answer the following questions: what is the difference between the left and right foot movement in EEG signals, whether it can be used as the identifiable feature to construct a classification model which can be applied in BCI systems. Ultimately, the findings of this study provide direct evidence that motor imagination and motor execution share similar mechanisms directly linked to lower limb motor action, meanwhile it offers a new classification model for the BCI system based on unilateral lower limb tasks.

4.1 | Disentangling cognitive components during real and imagined movements in two-foot controls — N100 and P300

There has been conflicting evidence as to whether the early ERP components include information on the locus of stimulus processing. N100 is an early component with no task-dependent changes to the lateralized presentation of stimuli [21, 22], but other studies have reported task-dependent changes as well [23, 24]. Our experimental results show that N^t1SF1 (TF6SF2) and N^t1SF2 (TF7SF2) were significantly different ($p<0.05$) with the effect of Side, which implies that N100 is a side-dependent component. Most previous studies agree that P300 involves multiple neural fields, such as occipital, temporal, parietal, frontal, thalamic, cerebellar, and limbic regions [25, 26]. Meanwhile, activated patterns of the underlying cortical regions are influenced by the type of stimulation and cognitive processing required by the particular task tested [27]. The hemispheric distribution of the P300 component may also be influenced by the parameters of the stimulus [28, 29]. This study also found that the asymmetry of TF2 and TF4 (P300) amplitude favored the unilateral hemisphere when lower limb movement with overt and covert actions was happening. Furthermore, the N100 and P300 components can be selected as the effective features in the classification model to verify its applicability in BCI.

4.2 | Feature extraction for BCI systems

The ERP-PCA method [30, 18] was used in this study for temporal-spatial feature extraction. Under the guidance of ERP-PCA analysis, the ERP-PCA components that can distinguish unilateral movement (left/right) formed the basis vectors of the matrix $\boldsymbol{W}$, which were used to extract potential ERP components from EEG signals for the classification of individual lower limb movement. As shown in Figure 6 and Table 3, more than half of the subjects achieved significant accuracy in both conditions, indicating that these ERP-PCA components of the single-trial of EEG signals are effective identifiable components.

It is easy to find that the significant feature sets of ME and MI are quite different, as shown in Figure 5, which

further indicates that unilateral lower limb movements under the two conditions lead to two different temporal-spatial patterns. The commonality of the significant feature sets of ME and MI is that they mainly cover P300 and N100 components. TP2 and TP3 component should be the main reason for the different classification results of MI and ME by observing the significant feature sets of ME and MI. Since the arrangement of ERP components followed the descending order of eigenvalues, TP2 and TP3 components were “larger” than that of P300 (TP4) and N100 (TP6 and TP7). The exploration of TP2 and TP3 components will be carried out in future studies.

Meanwhile, it is necessary to point out that the ERP-PCA classification model was not very prominent based on average accuracy. Due to the different mental states of each subject and possible noise, the performance of the proposed method for some subjects was not outstanding. Some studies [31, 32] mainly focus on the improvement of PCA algorithm, which can be further applied to our experiment. Therefore, it is very important to further improve the robustness of the feature extraction method.

5 | Limitations of this study

The neglect of our experimental design was the assessment of the participants' footedness. In addition, the exact onset of the motor tasks could not be ensured because the EMG of the foot was not detected. These limitations in the experimental design need to be addressed in further studies.

It was not difficult to found that a quarter of the participants had no significant classification result in both ME and MI, indicating that the classification features extracted from the spatiotemporal factor with statistical significance have serious individual differences. However, the same set of spatiotemporal factors was used for all subjects, which inevitably affected the classification accuracy for individuals. We need to find the spatiotemporal characteristics suitable for an individual to improve the classification accuracy.

6 | Conclusion

The high coincidence of ME and MI in spatiotemporal ERP components has indicated that the research result was consistent with the “functional equivalence” theory and provided the basis for the application of MI in BCI systems. Meanwhile, this study has revealed the temporal-spatial components for the left-right discrimination of unilateral foot motor imagery, and examined the role of ERP components in unilateral foot motor imagery recognition. Furthermore, the proposed ERP-PCA classification model can provide new strategies for improving lower limb BCI performance.

Acknowledgments

This work was supported by the National Social Science Fund of China under Grant 22BGL261.

References

[1] W.-Y. Hsu, EEG-based motor imagery classification using neuro-fuzzy prediction and wavelet fractal features, Journal of Neuroscience Methods 189 (2010) 295-302.

[2] N.F. Ince, A.H. Tewfik, S. Arica, Extraction subject-specific motor imagery time-frequency patterns for single trial EEG classification, Computers in Biology and Medicine 37 (2007) 499-508.

[3] G. Pfurtscheller, C. Neuper, C. Guger, W. Harkam, H. Ramoser, A. Schlogl, B. Obermaier, M. Pregenzer, Current trends in Graz Brain-Computer Interface (BCI) research, IEEE Transactions on Rehabilitation Engineering 8 (2000) 216-219.

[4] H. Berger, Über das elektroenkephalogramm des menschen, Archiv für Psychiatrie und Nervenkrankheiten 87 (1929) 527-570.

[5] N. Sharma, J.C. Baron, Does motor imagery share neural networks with executed movement: a multivariate fMRI analysis, Frontiers in Human Neuroscience 7 (2013).

[6] M. Jeannerod, Neural simulation of action: a unifying mechanism for motor cognition, Neuroimage 14 (2001) S103-S109.

[7] K. Amemiya, E. Naito, Importance of human right inferior frontoparietal network connected by inferior branch of superior longitudinal fasciculus tract in corporeal awareness of kinesthetic illusory movement, Cortex 78 (2016) 15-30.

[8] S. Glover, M. Baran, The motor-cognitive model of motor imagery: evidence from timing errors in simulated reaching and grasping, Journal of Experimental Psychology. Human Perception and Performance 43 (2017) 1359-1375.

[9] S. Glover, E. Bibby, E. Tuomi, Executive functions in motor imagery: support for the motor-cognitive model over the functional equivalence model, Experimental Brain Research 238 (2020) 931-944.

[10] S. Mathews, P.J.A. Dean, A. Sterr, EEG dipole analysis of motor-priming foreperiod activity reveals separate sources for motor and spatial attention components, Clinical Neurophysiology 117 (2006) 2675-2683.

[11] T. Hanakawa, M.A. Dimyan, M. Hallett, Motor planning, imagery, and execution in the distributed motor network: a time-course study with functional MRI, Cerebral Cortex 18 (2008) 2775-2788.

[12] E. Hernandez-Martin, F. Marcano, C. Modrono, N. Janssen, J.L. Gonzalez-Mora, Diffuse optical tomography to measure functional changes during motor tasks: a motor imagery study, Biomedical Optics Express 11 (2020) 6049-6067.

[13] J. Packheiser, J. Schmitz, G. Berretz, D.P. Carey, S. Paracchini, M. Papadatou-Pastou, S. Ocklenburg, Four meta-analyses across 164 studies on atypical footedness prevalence and its relation to handedness, Scientific Reports 10 (2020) 14501.

[14] L. Gu, Z. Yu, T. Ma, H. Wang, Z. Li, H. Fan, EEG-based classification of lower limb motor jmagery with brain network analysis, Neuroscience 436 (2020) 93-109.

[15] H. Yasunari, U. Junichi, EEG-based classification of imaginary left and right foot movements using beta rebound, Clinical Neurophysiology Official Journal of the International Federation of Clinical Neurophysiology 124 (2013) 2153-2160.

[16] A. Delorme, S. Makeig, EEGLAB: an open source toolbox for analysis of single-trial EEG dynamics including independent component analysis, Journal of Neuroscience Methods 134 (2004) 9-21.

[17] J. Dien, The ERP PCA Toolkit: an open source program for advanced statistical analysis of event-related potential data, Journal of Neuroscience Methods 187 (2010) 138-145.

[18] J. Dien, C.A. Michelson, M.S. Franklin, Separating the visual sentence N400 effect from the P400 sequential expectancy effect: cognitive and neuroanatomical implications, Brain Research 1355 (2010) 126-140.

[19] V. Bajaj, R.B. Pachori, Classification of Seizure and Nonseizure EEG Signals Using Empirical Mode Decomposition, IEEE Transactions on Information Technology in Biomedicine 16 (2012) 1135-1142.

[20] N. Nicolaou, J. Georgiou, Detection of epileptic electroencephalogram based on permutation

entropy and support vector machines, Expert Systems with Applications 39 (2012) 202-209.
[21] A. Kok, J.A.J. Rooyakkers, ERPs to laterally presented pictures and words in a semantic categorization task, Psychophysiology 23 (1986) 672-683.
[22] S.R. Schweinberger, W. Sommer, R.M. Stiller, Event-related potentials and models of performance asymmetries in face and word recognition, Neuropsychologia 32 (1994) 175-191.
[23] A. Nowicka, A. Grabowska, E. Fersten, Interhemispheric transmission of information and functional asymmetry of the human brain, Neuropsychologia 34 (1996) 147-151.
[24] V.J. Samar, Multidimensional influences of cerebral asymmetries on visual half-field asymmetries and cognitive skills, Brain and Cognition 2 (1983) 355-382.
[25] J.M. Clarke, E. Halgren, P. Chauvel, Intracranial ERPs in humans during a lateralized visual oddball task: II. Temporal, parietal, and frontal recordings, Clinical Neurophysiology 110 (1999) 1226-1244.
[26] K.A. Moores, C.R. Clark, J.L.M. Hadfield, G.C. Brown, D.J. Taylor, S.P. Fitzgibbon, A.C. Lewis, D.L. Weber, R. Greenblatt, Investigating the generators of the scalp recorded visuo-verbal P300 using cortically constrained source localization, Human Brain Mapping 18 (2003) 53-77.
[27] A. Mecklinger, B. Maess, B. Opitz, E. Pfeifer, D. Cheyne, H. Weinberg, A MEG analysis of the P300 in visual discrimination tasks, Evoked Potentials-Electroencephalography and Clinical Neurophysiology 108 (1998) 45-56.
[28] J. Kayser, G.E. Bruder, C.E. Tenke, J.W. Stewart, F.M. Quitkin, Event-related potentials (ERPs) to hemifield presentations of emotional stimuli: differences between depressed patients and healthy adults in P3 amplitude and asymmetry, International Journal of Psychophysiology 36 (2000) 211-236.
[29] A.M. Proverbio, A. Zani, Electrophysiological indexes of illusory contours perception in humans, Neuropsychologia 40 (2002) 479-491.
[30] J. Dien, Evaluating two-step PCA of ERP data with Geomin, Infomax, Oblimin, Promax, and Varimax rotations, Psychophysiology 47 (2010) 170-183.
[31] I. Razzak, I.A. Hameed, G. Xu, Robust sparse representation and multiclass support matrix machines for the classification of motor imagery EEG signals, IEEE Journal of Translational Engineering in Health and Medicine 7 (2019).
[32] L.-C. Shi, R.-N. Duan, B.-L. Lu, IEEE, A robust principal component analysis algorithm for EEG-based vigilance estimation. 35th Annual International Conference of the IEEE-Engineering-in-Medicine-and-Biology-Society (EMBC), Osaka, JAPAN, 2013, pp. 6623-6626.